

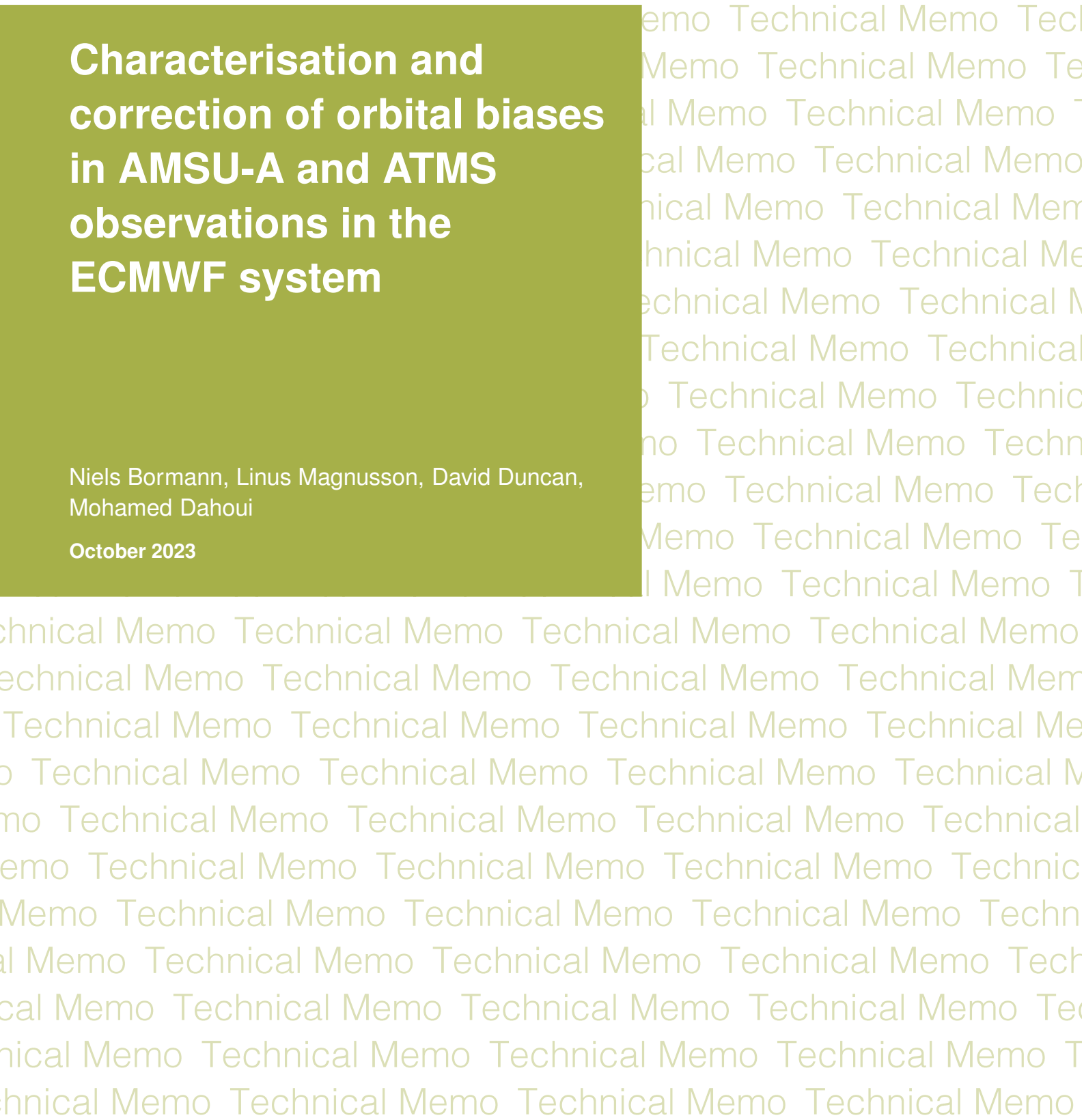
Technical Memo

912

Characterisation and correction of orbital biases in AMSU-A and ATMS observations in the ECMWF system

Niels Bormann, Linus Magnusson, David Duncan,
Mohamed Dahoui

October 2023



Series: ECMWF Technical Memoranda

A full list of ECMWF Publications can be found on our web site under:
<http://www.ecmwf.int/en/publications/>

Contact: library@ecmwf.int

© Copyright 2023

European Centre for Medium Range Weather Forecasts, Shinfield Park, Reading, RG2 9AX, UK

Literary and scientific copyrights belong to ECMWF and are reserved in all countries. The content of this document is available for use under a Creative Commons Attribution 4.0 International Public License.

See the terms at <https://creativecommons.org/licenses/by/4.0/>.

The information within this publication is given in good faith and considered to be true, but ECMWF accepts no liability for error or omission or for loss or damage arising from its use.

Abstract

This study investigates orbital biases in passive microwave (MW) temperature-sounding observations in the 50-60 GHz band by comparing observations against the ECMWF background. Methods to correct for the biases by modifying the model used in the variational bias correction are also examined.

The analysis suggests that there are considerable orbital biases in MW temperature-sounding observations from AMSU-A and ATMS, with a distinct seasonal cycle, and magnitudes that can reach levels comparable in size to the instrument noise (0.1-0.2 K). The largest orbital biases occur during June-October, and they lead to systematic diurnal increments in the ECMWF analysis over the Southern Hemisphere. All AMSU-A instruments exhibit similar bias patterns, despite different equator-crossing times, albeit with some variation in the magnitude. NOAA-18 AMSU-A shows the strongest biases. Further analysis suggests that the bias is observation-related, rather than a bias in the background.

Assimilation experiments show that the orbital biases can be addressed within the variational bias correction by adding terms based on a Fourier-series in the orbital angle to the bias correction model, following Booton et al (2013). This leads to a significant reduction of the systematic diurnal increments, with minor benefits in the short-range forecasts up to day 2. Care has to be taken to limit the additional degrees of freedom introduced through the modified bias correction, to avoid over-fitting of the biases and interactions with model biases in the stratosphere. To limit these effects, the use of an “alternating Fourier series” as bias model is proposed, together with not applying the modified bias model to the highest stratospheric channels.

Plain language summary

This study looks at systematic differences between satellite observations and equivalent values simulated from short-range forecasts made with the ECMWF forecasting system. The observations investigated measure radiation emitted by the Earth’s atmosphere in the microwave part of the electromagnetic spectrum and provide important information on temperature layers in the atmosphere. We find that for certain times of the year, there are sizeable systematic differences that depend on where the satellite is positioned around its sun-synchronous orbit. The differences are largest during June-October, for the part of the orbit where the satellite is located over the Southern Hemisphere. The difference pattern are similar for a range of satellites, with some variation in magnitude, but no clear dependence on the local time-of-day the satellites observe. Further investigation suggest that the differences are likely due to errors in the observations or how we simulate them, rather than due to systematic errors in the short-range forecasts. The systematic differences around the orbit are currently not corrected when the observations are used to calculate initial conditions for our weather forecasts. This results in spurious systematic diurnal pattern in the initial conditions.

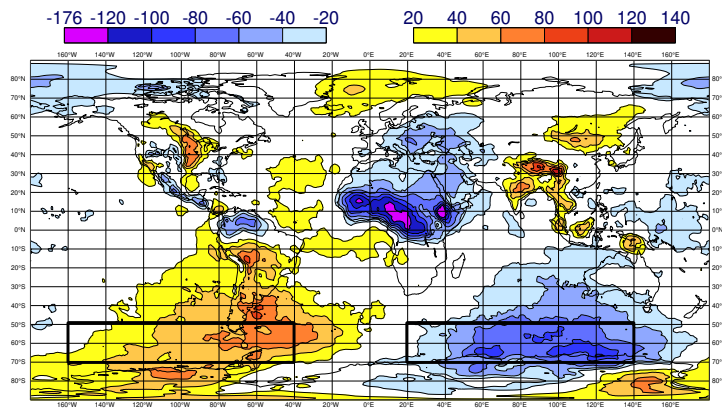
We show that approaches based on Booton et al (2013) can be used to successfully correct for the systematic differences around the orbit. This leads to minor benefits in the short-range forecasts up to day 2. Care has to be taken to avoid that the correction erroneously corrects for other systematic errors in the assimilation system, such as from the forecast model. To achieve this, the correction is applied only to selected channels, and we use a variant of the correction originally developed by Booton et al (2013).

1 Introduction

This study investigates orbital biases seen in differences between observations and background equivalents for passive microwave (MW) temperature-sounding observations in the 50 GHz band from polar-orbiting satellites in the ECMWF assimilation system, and explores ways to address these biases as part of the variational bias correction. MW temperature-sounding in the 50-GHz band is currently available from instruments such as AMSU-A and ATMS, and these are flown on a range of polar-orbiting platforms from the US and Europe (NOAA, Metop, and JPSS series of satellites). Observations from these instruments have been available for several decades, and they remain one of the main contributors to the skill of global numerical weather forecasts and climate reanalyses (e.g., Bormann et al 2019, Hersbach et al 2020), not least as they provide temperature-information with good coverage in all-sky conditions.

The present study was prompted by the finding that the operational ECMWF assimilation system exhibits systematic diurnal thickness increments during certain times of the year. These can be seen in maps of differences in the mean analysis increment between the 12Z and the 00Z assimilation cycles (Fig. 1).

(a) June - August 2020



(b) December 2020 - February 2021

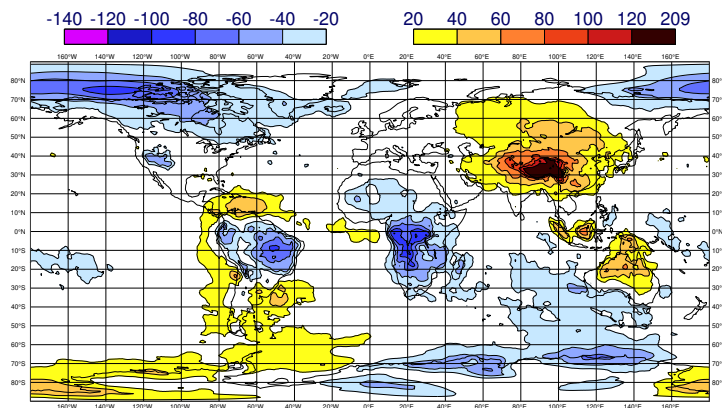


Figure 1: Difference in the mean increments between the 12Z and the 0Z cycle for the 925-200 hPa geopotential thickness [m^2/s^2] for June-August 2020 (a) and December 2020 - February 2021 (b), taken from the operational ECMWF system. The two areas marked in panel a) are 40-160°W/50-70°S and 20-140°E/50-70°S, and they are used for statistics shown in Fig. 2.

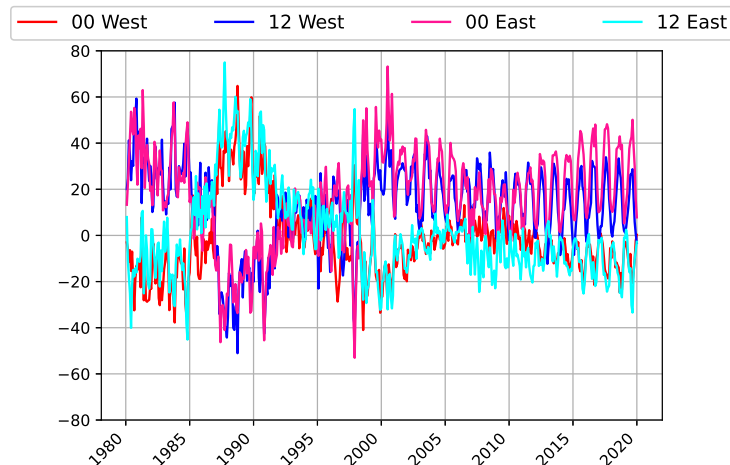


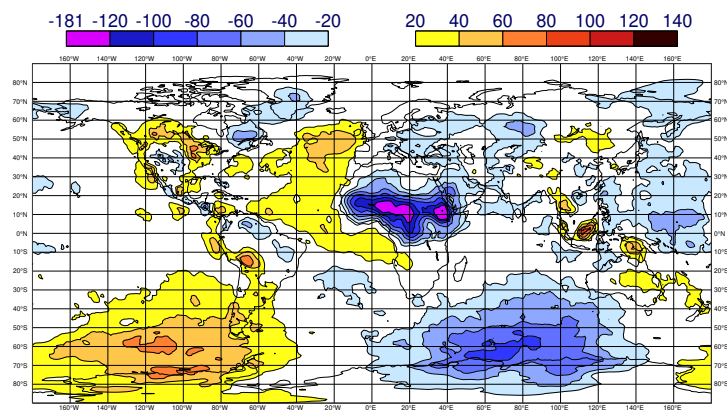
Figure 2: Time series of the mean increments for the 925-200 hPa geopotential thickness [m^2/s^2] over selected geographical areas, taken from the ERA5 reanalysis. The geographical areas are $40\text{-}160^\circ\text{W}/50\text{-}70^\circ\text{S}$ (“West”) and $20\text{-}140^\circ\text{E}/50\text{-}70^\circ\text{S}$ (“East”), and they are depicted in Fig. 1a. The different lines show results for the 0Z and 12Z cycle, respectively, as indicated in the legend.

During the June-August season, systematic differences are present over the Southern-Hemisphere mid-latitudes, with values exceeding $80 \text{ m}^2/\text{s}^2$ in places. A similar, albeit weaker pattern is found for the Northern-Hemisphere high latitudes, during December-February. Note that ECMWF uses a 12-hour assimilation window, and the differences in the 12Z and 00Z mean increments hence result from the assimilation of observations from 9-21Z and 21-9Z, respectively. The diurnal increments are also present in the ERA5 reanalysis (Hersbach et al 2020), as illustrated in Fig. 2. The Figure shows timeseries of the mean increments in the two geographical regions marked in Fig. 1a over the Southern Hemisphere. There are systematic increments with a clear seasonal pattern from the late 1990s onwards, coinciding with the advent of ATOVS observations (e.g., McNally and Kelly 1999). The magnitude of the increments varies over the years, with a minimum around 2008, but the seasonal pattern is relatively stable. Systematic increments of a similar size are also present prior to the advent of ATOVS data, with a less clear and stable seasonal pattern and a reversal in sign between 1985 and 1994.

Further investigations show that the diurnal increment patterns at mid-latitudes largely disappear when MW sounding observations are excluded from the assimilation system (cf Fig. 3 a and b). Some systematic diurnal increments remain over the Tropics, likely the result of the analysis correcting model-biases linked to convective activity. The systematic increments over the mid-latitudes seen in the full system could of course also be the result of the analysis correcting diurnal model biases in other aspects of the forecast model. But the finding that the systematic increment patterns disappear in the absence of MW-sounding observations makes this less likely, as it would mean that MW-sounding observations were the only observing system able to detect and correct for such biases, whereas observing systems such as hyperspectral infrared (IR) instruments or GNSS radio occultation clearly have relevant sensitivity to such a bias. This provides some indication that the diurnal increments are caused by the MW-sounding observations themselves or our usage of them.

Diurnal biases in satellite observations from sun-synchronous orbit can be caused by orbital biases, that is, biases that are linked to the space-craft’s position within the orbit in a systematic and repeatable way. Orbital biases are a common feature in conically scanning MW imagers (e.g., Scanlon et al 2023, Geer et al 2010, Bell et al 2008). They are often linked to varying illuminations of the instrument by the sun

(a) Control



(b) MW sounder denial

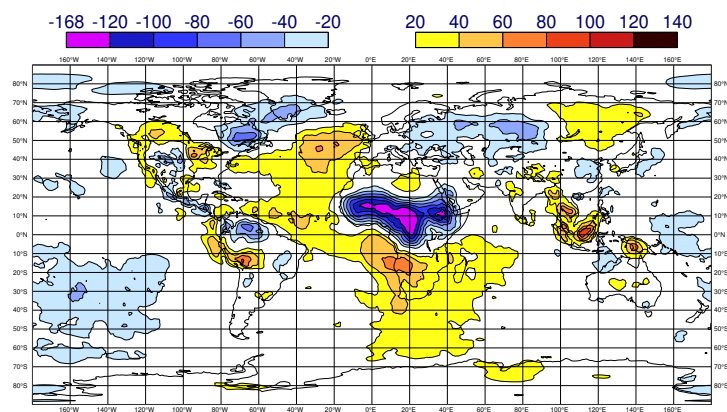


Figure 3: As Fig. 1a, but taken from the lower-resolution observing system experiments discussed in Bormann et al (2019) for the period June-August 2016. Panel a) shows results from a Control experiment that uses the full observing system, whereas panel b) shows results from an experiment in which all MW sounding observations have been denied.

around the orbit and the thermal variations resulting from that. Conical scanners require a relatively large exposed reflector, and any emission signatures of this reflector are difficult to take fully into account in the calibration. Biases due to thermal variations in the reflector temperatures, combined with an emissive reflector, have been observed, for instance, for SSMIS, TMI, and MWRI (e.g., Bell et al 2008, Geer et al 2010, Xie et al 2019). The amplitude of such biases can reach several K, depending on the channel. Other sources of orbital biases observed for SSMIS have been solar intrusions into the warm calibration load, leading to incorrect calibration for the affected parts of the orbit (Bell et al 2008). In all of these studies, comparisons of the observations against model equivalents calculated from short-range forecasts have provided important insights into detecting and correcting the observed biases. Orbital biases in cross-track scanners such as AMSU-A and ATMS have, to our knowledge, not yet been reported. Orbital biases for these instruments are less likely, as the more compact instrument design allows that signatures due to reflector emissions can be taken into account during the calibration process, thus eliminating one source of such bias.

While orbital biases for cross-track sounders may be expected to be smaller than for conical-scanners, the accuracy requirements for the temperature-sounding channels on these instruments are considerably

higher. The typical size of random errors in the forecast background for the tropospheric temperature-sounding channels is around 0.1 K (Bormann and Bauer 2010), with instrument noise values for the assimilated observations typically around 0.1-0.2 K (after super-obbing in the case of ATMS). To assimilate the observations effectively, observational biases need to be corrected to sufficiently small levels, in order to be able to correct for the random errors in the background. At ECMWF this is performed using Variational Bias Correction (VarBC, Dee 2004), relying on adequate models to represent the bias. However, if bias features are present in the observations or the observation operator that the bias model does not capture, then these will result in a residual bias.

In the present paper, we present a detailed analysis of orbital biases in AMSU-A and ATMS observations. To our knowledge, such biases have not previously been investigated. We establish that these orbital biases are the cause for the systematic diurnal increments in the ECMWF system and investigate ways to correct for the bias. The structure of the paper is as follows. We will first characterise residual orbital biases found in comparisons between AMSU-A and ATMS observations against the ECMWF background. We will provide further indications that they are an observation-related bias. This will be followed by an investigation into addressing the orbital biases by modifying the bias model used in VarBC for selected channels. Conclusions from this work are summarised in the final section.

2 Characteristics of the orbital biases

Orbital biases in sounding channels of AMSU-A and ATMS are investigated in this paper by comparing brightness temperature observations against equivalent values calculated from model background using the RTTOV radiative transfer model (Saunders et al 2018). Unless indicated otherwise, bias statistics will be based on differences between observations and model backgrounds (“background departures”) after bias correction, and we will refer to these as “residual bias”. Observational biases in level 1 brightness temperatures are corrected in the ECMWF system using VarBC (Dee 2004). This relies on an adequate parameterised model for the observational bias, and it estimates the free parameters of this bias model during the assimilation alongside performing the geophysical analysis. The bias model used for the MW sounders consists of a global constant, a model to capture air-mass biases, and a scan-bias model (e.g., Duncan et al 2022, Bormann et al 2013). The air-mass model is a linear model that uses four layer-thicknesses from the background as predictors (100-300 hPa, 200-50 hPa, 50-5 hPa, and 10-1 hPa), whereas the scan-bias model uses a third-order polynomial in the scan-angle. This bias model has been found to address most of the typically encountered observational biases adequately. However, it is clear that this model will be unable to capture orbital biases, such as different biases in the ascending or

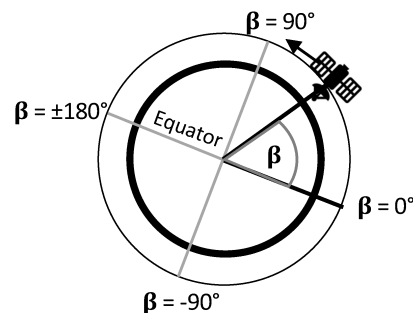


Figure 4: Schematic of the definition of the orbital angle β used in this study.

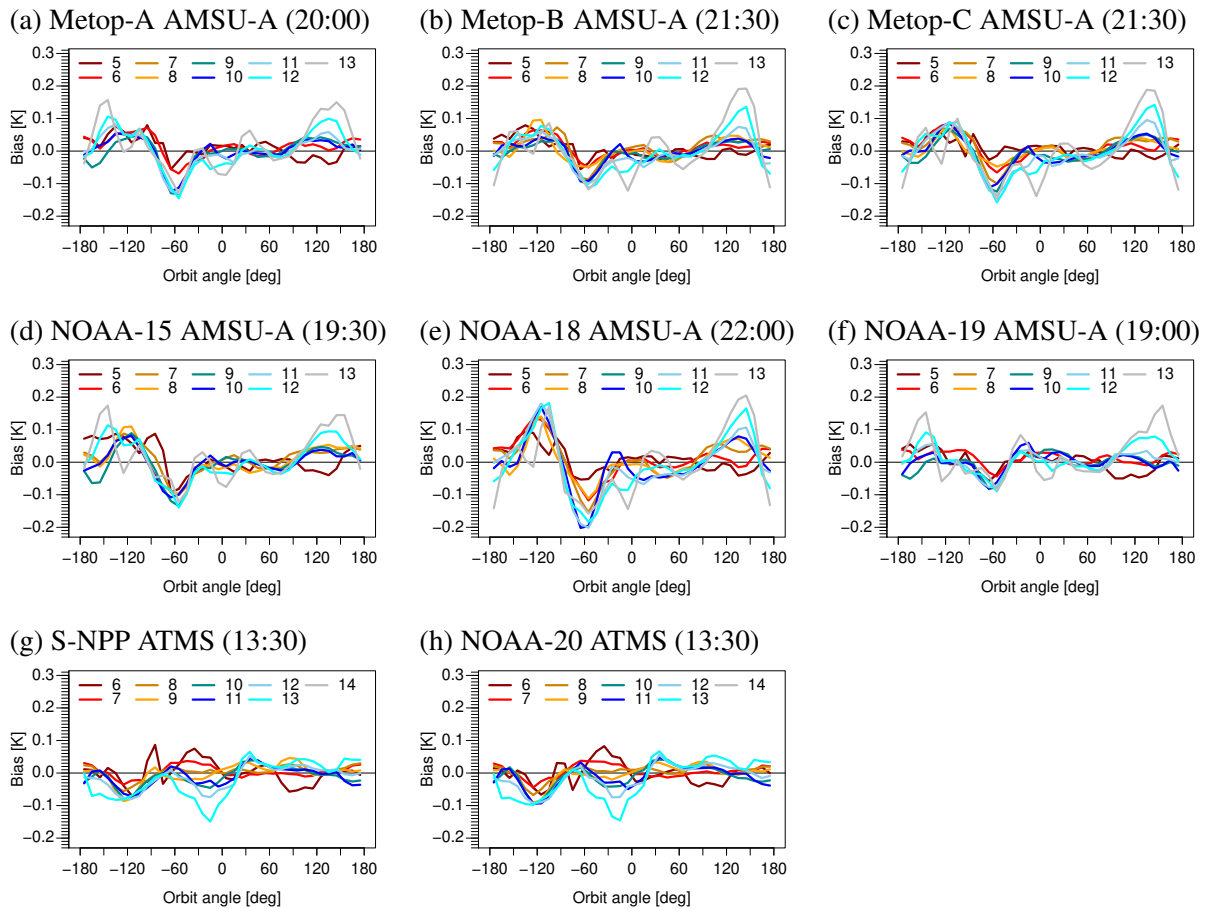


Figure 5: Residual bias [K] as a function of orbital angle for August 2021 for the sounding channels used in the assimilation system for AMSU-A and ATMS instruments on various satellite platforms. See the colour legend for the channel number. Statistics are taken from the ECMWF operational high-resolution system. The numbers in brackets give the approximate local time ascending node for each satellite.

descending node of the orbit, as no bias predictor is included that would allow capturing such biases.

To characterise the orbital biases in this paper we use an orbital angle β which gives the position of the satellite in the orbital plane. It is defined here for polar-orbiting satellites as the angle given by the satellite’s position, the centre of the Earth, and the intersection of the ascending node of the orbit and the equatorial plane, as depicted schematically in Fig. 4. The orbit angle is 0° when the satellite ascends over the equator and $\pm 180^\circ$ when it descends over the equator, with positive orbit angles positioned over the Northern Hemisphere and negative orbit angles over the Southern Hemisphere. Orbit angles of $\pm 90^\circ$ indicate the place in the orbit where the satellite is positioned closest to the poles. Note that other definitions of the orbit angle have been used, for instance, by Booton et al (2013) who define an orbital angle relative to the ecliptic plane. The definition used here is instead independent of the relative position of the sun, and this makes the translation between orbit angle and viewed latitudes easier.

Figure 5 shows considerable residual biases for the AMSU-A and ATMS sounding channels as a function of the orbit angle for the month of August 2021. The NOAA-18 AMSU-A exhibits the strongest biases, with magnitudes reaching ± 0.2 K, whereas values up to ± 0.1 K are more typical for other instruments. While these values may appear small, they are nevertheless sizeable compared to the instrument noise values of around 0.15-0.2 K for these channels and the random component of errors in the model back-

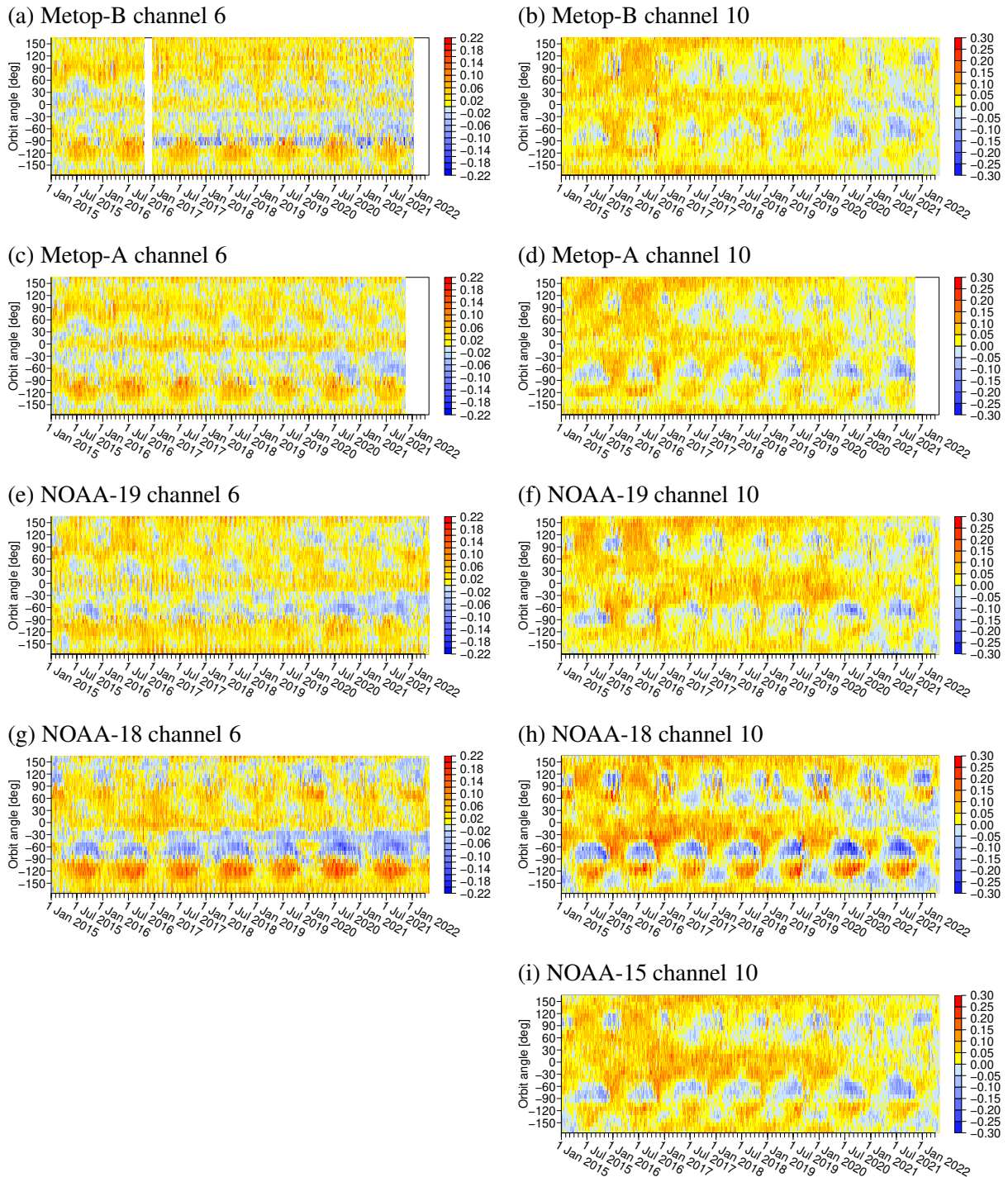


Figure 6: Residual bias [K] as a function of date (x-axis) and the orbital angle (y-axis) for selected AMSU-A channels, with statistics calculated from used data from the ECMWF operational high-resolution system. Statistics are shown for every 5th day, with separate colour points for each 0 and 12 Z assimilation cycle. Results for AMSU-A channel 6 are shown in the left column, whereas results for channel 10 are displayed in the right column. Different rows refer to instruments on different satellites, as indicated in the panel heading. Channel 6 on NOAA-15 has failed and is hence not shown.

ground of around 0.1 K (e.g., Bormann and Bauer 2013). For AMSU-A, most of the sounding channels show remarkably consistent bias pattern, with peaks around $\beta = -120^\circ$, -60° and 140° . Note that the presence of any residual zonally-dependent air-mass biases would lead to bias structures that are locally symmetric around orbital angles of $\pm 90^\circ$, the orbit-angles for which the satellite is closest to the poles. In contrast, the peaks around -120° and -60° have opposite signs and therefore cannot be due to zonally-dependent air-mass biases. Instead, they reflect biases of opposing sign affecting similar mid-latitudes over the Southern Hemisphere over the descending and ascending part of the orbit, respectively. The peak around $\beta = 140^\circ$ affects the Northern Hemisphere mid-latitudes over the descending part of the orbit. Even though the magnitudes vary, the patterns are strikingly consistent between the instruments on the different satellites, despite very different equator crossing times. For ATMS, some orbital biases are also visible (Fig. 5g and h), but the magnitude is smaller and the patterns are different from the ones seen for AMSU-A.

The orbital bias shows a complex seasonal pattern that is relatively consistent over a period of 7 years, as shown in Fig. 6. The dipole structure of biases for negative orbit angles noted in Fig. 5 is strongest during June-October. A similar but fainter bias dipole exists for positive orbit angles, and this is strongest during December through to February.

The stability of the seasonal pattern over the 7-year period is remarkable, as neither the ECMWF system nor the constellation of the satellites shown was stable during the period shown. The operational ECMWF system has undergone a number of changes during these 7 years, with modifications approximately every year, affecting both the assimilation and forecast model. This includes, for instance, the move of AMSU-A from clear-sky to all-sky assimilation (in October 2021, Duncan et al 2022). It appears, however, that the patterns are mostly unaffected by these changes to the ECMWF system. The only exception is a change to the treatment of model-biases, affecting primarily the stratosphere. This was introduced in cycle 47r1 on 13 July 2020, and the effect is visible in Fig. 6 as an overall shift of the residual bias around this time for all satellites. However, even more remarkable is the consistency of the seasonal bias patterns between the AMSU-A instruments on different satellites, despite their different equator crossing times which, in the case of the NOAA satellites, changed significantly during the period shown (Fig. 7). The local time ascending node (LTAN) for NOAA-18, for instance, has changed from 16:30 in 2015 to 22:00 in 2022. This means the ascending node for NOAA-18 has moved from covering

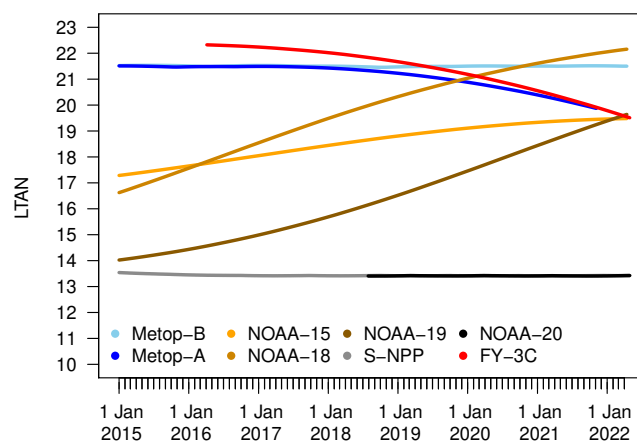


Figure 7: Local time ascending node (LTAN) for the satellites considered in this study. Metop-C is not shown, but follows the LTAN of Metop-B.

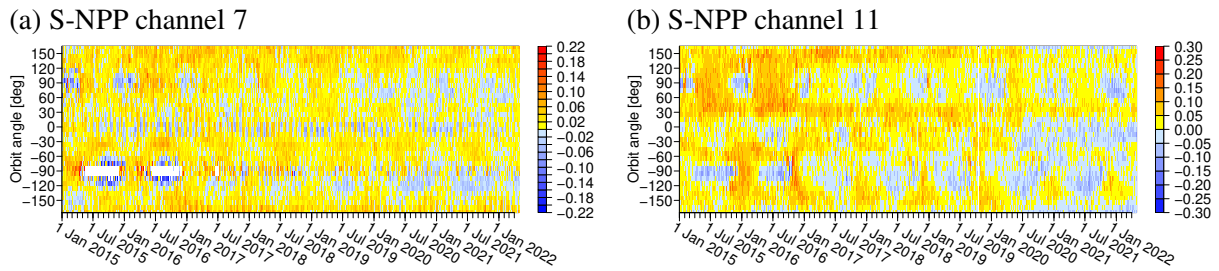


Figure 8: As Fig. 6, but for ATMS on S-NPP. The two panels show channels 7 and 11, respectively, which are equivalent to AMSU-A channel 6 and 10 shown in Fig. 6.

day-time in 2015 to night-time in 2022. It also means that the thermal environment and cycling of the satellite has changed completely during this time. However, these changes have not affected the seasonal pattern observed in the residual bias. We will get back to these points when we discuss the likely origin of the biases.

The temporal evolution of the orbital biases for ATMS is also relatively stable, at least from around mid-2017 onwards (Fig. 8). Some different patterns are visible prior to this, likely due to an upgrade to the calibration implemented in the ATMS processing in March 2017¹ and a modification of the ATMS data usage over land and sea-ice in the ECMWF system in July 2017, affecting channel 7. While the patterns are different, it is noticeable that the clearest orbital biases are again occurring around June-October for negative orbital angles (Southern Hemisphere) and around December-February for positive orbital angles (Northern Hemisphere).

The dipoles in the orbital biases and the seasonal pattern are consistent with the occurrence of the systematic increment pattern highlighted in Fig. 1. Due to the nature of the sun-synchronous polar orbits, the dipole pattern around $\pm 90^\circ$ in the residual bias as a function of orbit angle means that the latitude regions with negative biases during one 12-hour cycle will experience a positive bias during the next 12-hour cycle. The resulting difference in the bias between the 12Z and the 0Z cycle is highlighted in a geographical map in Fig. 9 for channel 10 for the different instruments. All these difference maps are showing clear East/West pattern that are determined by whether we are taking the difference in bias between the ascending and the descending part of the orbit or vice versa. Channel 10 is shown here because the channel is functioning well for all instruments assimilated, but other channels show a qualitatively similar pattern. It turns out that the AMSU-A instruments are all exhibiting a similar geographical pattern in these 12Z-0Z bias differences over the Southern Hemisphere during this time. As a result, the analysis responds by producing systematic increments that are different between the 12Z and the 0Z cycle throughout the troposphere and the stratosphere, and they are a compromise between the bias information provided by the different instruments. The consistency with the locations of the largest diurnal increment differences over the Southern Hemisphere shown in Fig. 9 for this season is striking.

A few aspects noted so far suggest that the orbital biases are not the result of biases in the background, but rather arise from the observations themselves, the observation operator, or our usage of the observations. This includes the finding that the systematic diurnal increments are not present in the ECMWF system when the MW sounders are denied (Fig. 3), combined with the clear link between the geographical pattern of the diurnal increments and the residual biases (Fig. 9). Similarly, while different AMSU-A and ATMS instruments exhibit qualitatively similar residual biases, the magnitudes of the diurnal biases

¹The move from the “block1.2” to the “block2.0” in the NESDIS processing included updates to the non-linearity correction, as well as a move to performing the calibration in terms of radiances (rather than brightness temperatures), with a final conversion to brightness temperatures using the full Planck equation.

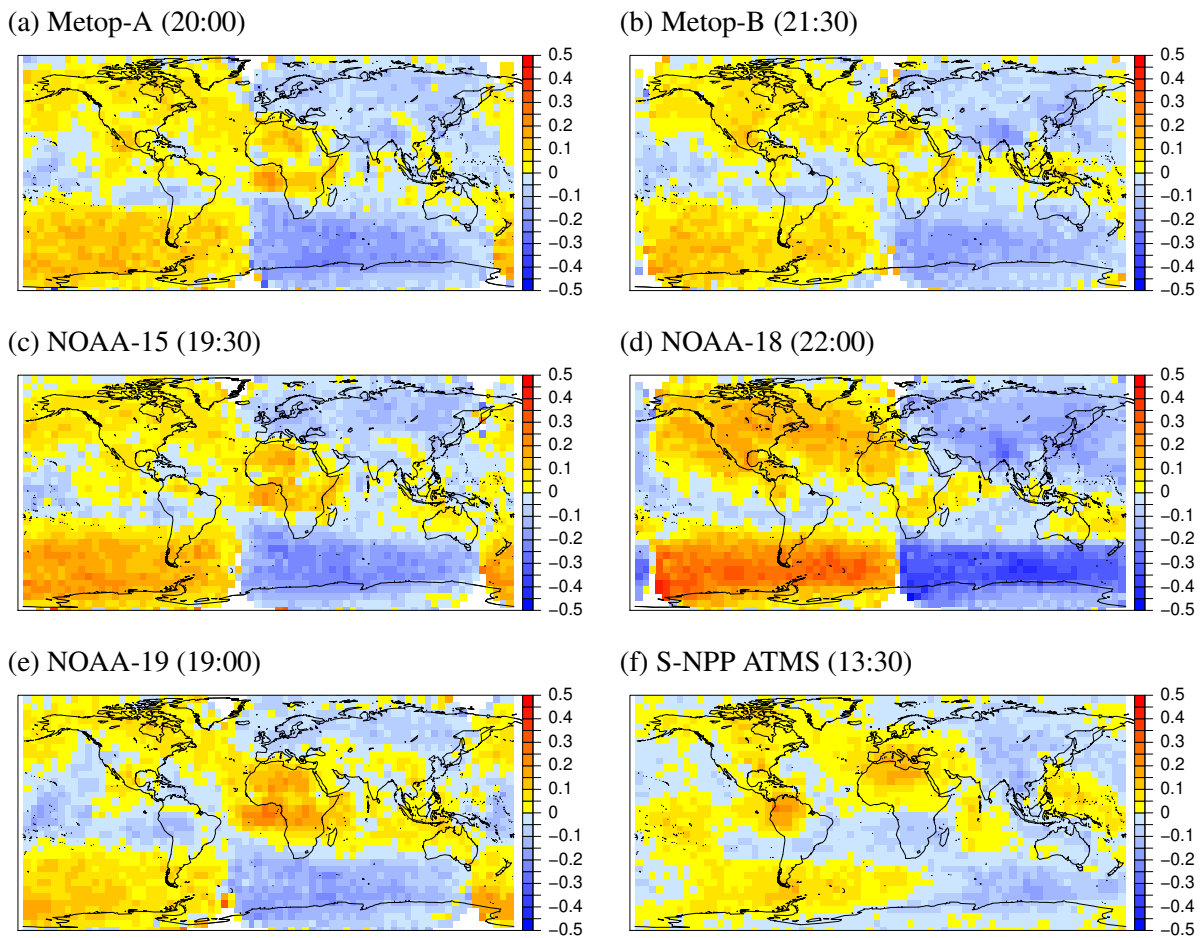


Figure 9: Difference between the mean residual bias in the observations used in the 12 Z cycle and the ones used in the 00 Z cycle. Statistics are for channel 10 of AMSU-A (a-e) and channel 11 of ATMS (f) calculated from the operational ECMWF system for July 2021. The satellites are given in the panel heading, together with the LTAN in brackets.

are different even for instruments that sense at similar overpass times (cf NOAA-18 and Metop-A in Fig. 9). This would not be the case if the statistics were driven by a bias in the background. Similarly, other temperature-sensitive radiance observations peaking at similar altitudes also do not show similar orbital biases (see appendix A.1), further indicating that the bias is specific to the AMSU-A and ATMS temperature-sounding channels.

The root cause of the orbital bias remains unclear, but it is likely related to neglected in-orbit variations in the calibration of the instruments. An effect linked to the thermal environment of the instrument or the satellite itself appears less likely, given that the seasonal bias patterns for all satellites are very stable, even though the equator-crossing time has changed very significantly over the period considered for some satellites (e.g., NOAA-18). In line with this, no clear link has been found between the orbital bias pattern and the instrument temperatures recorded with the data around the orbit (not shown). Some further analysis of bias characteristics are presented in appendix A.2, aimed at providing clues towards the root cause, but a clear identification remains elusive and is considered beyond the scope of the present work.

3 Correcting the orbital bias in VarBC

3.1 Method

Having established that the residual biases seen for AMSU-A and ATMS data are most likely observation-related, we will now experiment with ways to correct the bias through a modification of the bias-correction model used in VarBC. Following Booton et al (2013), we explore here the use of a bias model based on a Fourier-series in the orbital angle. That is, the orbital bias is modelled by adding the following to the bias correction model:

$$b(\beta) = \sum_{i=1}^n (a_i \cos(i\beta) + b_i \sin(i\beta)) \quad (1)$$

Here, a_i and b_i are the Fourier expansion coefficients, and n is a number chosen so that the residual bias is sufficiently captured. When applying this model to SSMIS data, Booton et al (2013) found $n = 5$ to be a suitable compromise between adequately fitting the bias and limiting the number of free parameters. Offline experimentation with different choices of n showed that this is also an adequate choice to fit the residual orbital biases seen here for AMSU-A and ATMS for most periods (not shown). Occasionally, sharper changes in the bias with orbital angle are not fully captured, and fitting such features would require a higher order Fourier series to be used.

As noted by Booton et al (2013), the above bias model can be easily implemented in VarBC. The terms $\sin(i\beta)$ and $\cos(i\beta)$ become additional bias predictors in VarBC, and a_i and b_i represent the bias parameters that will be estimated as part of performing the atmospheric analysis. With $n = 5$, this means that 10 additional bias parameters are added for each channel and instrument treated for which the orbital bias correction is applied.

The choice of bias models in VarBC is always a trade-off between adequately modelling biases, but also ensuring that the bias parameters are well-constrained and focus on the observational bias to be corrected. A draw-back of the above bias model in this context is that it adds a relatively large number of bias parameters. For most AMSU-A channels, the current operational bias model uses 8 bias parameters per channel (four for the air-mass correction based on four layer thicknesses, three for a 3rd-order polynomial in the scan-angle for the scan-bias, and one global constant). The 5-th order Fourier series hence more than doubles the number of bias parameters for these channels. In addition, the 5-th order Fourier series allows modelling of biases with zonal structure: This can be seen in Fig. 10a and b which show the predictors or Fourier basis functions used. Predictors that are locally symmetric around $\beta = \pm 90^\circ$ will allow the correction of biases with zonal structure (e.g., the $\sin(\beta)$ predictor shown as black line in Fig. 10a, or the $\cos(2\beta)$ predictor shown as grey line in Fig. 10b). Biases with zonal structure may be air-mass dependent biases (e.g., arising from radiative-transfer biases) which are already supposed to be addressed through the existing air-mass predictors. They may also be characteristics of model biases. As will be seen later, this situation can lead to over-fitting of air-mass dependent biases.

To address these issues, we are also experimenting with an alternative bias correction model that is designed to avoid the correction of biases with zonal structure. To do so, we exclude any terms of the Fourier series that allow zonal structure, that is, any terms that are locally symmetric around $\beta = \pm 90^\circ$, as follows:

$$b_{\text{Alt}}(\beta) = a_1 \cos(\beta) + b_2 \sin(2\beta) + a_3 \cos(3\beta) + b_4 \sin(4\beta) + a_5 \cos(5\beta) + b_6 \sin(6\beta) \quad (2)$$

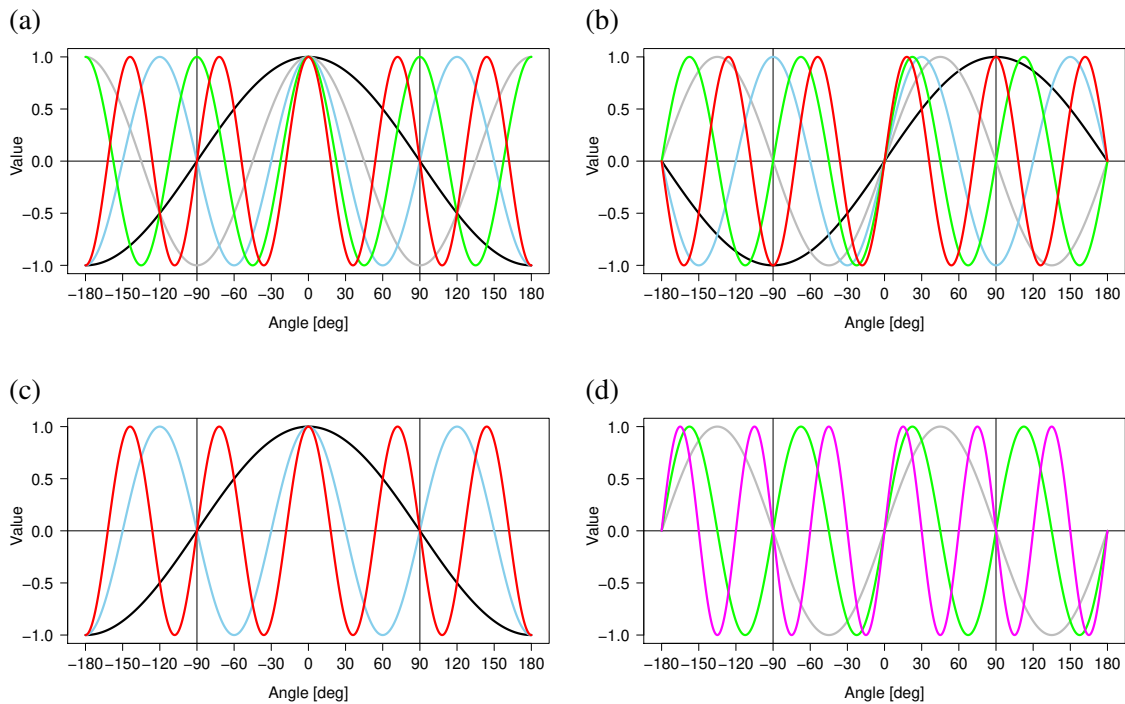


Figure 10: Basis functions of the Fourier series expansions used in the bias correction models. Panels (a) and (b) show the cos and sin functions of the full 5th-order Fourier series used, respectively, whereas (c) and (d) show the cos and sin functions of the alternating Fourier series, respectively.

We will refer to this model as the “alternating Fourier-series”, as it alternates between the cos and sin terms of the usual Fourier series. To allow an even number of cos and sin terms, $\sin(6\beta)$ is added as predictor compared to the 5-th order Fourier series introduced above. The resulting model uses only 6 predictors, and offline experimentation with fitting this bias model to the observed residual biases suggests that it nevertheless captures most of the structure of the residual bias. The predictors (or basis functions) are depicted in Fig. 10c and d.

3.2 Experiments

A set of assimilation experiments has been conducted to test the orbital bias correction approach as in Booton et al (2013), as well as the more selective bias correction based on the alternating Fourier series. For the alternating Fourier series, several experiments are performed that apply the bias correction to different sets of channels. These aim to further reduce interaction with model bias in the stratosphere by excluding the top-most channels from the orbital bias correction. They also test extending the orbital bias correction to the lowest sounding channel for which the correction was initially not included due to concerns that biases arising from the surface treatment may alias into the orbital bias correction, particularly over land and sea-ice.

Control: An experiment that uses all observations in a similar way as the present operational ECMWF system. It uses the standard bias correction models for AMSU-A and ATMS.

FourierCh6-13: As Control, but the bias correction model for AMSU-A channels 6 - 13 and the equiv-

alent ATMS channels 7 - 14 is modified by adding a 5-th order Fourier series in the orbital angle.

AltFourierCh6-13: As Control, but the bias correction models for AMSU-A channels 6-13 and the equivalent ATMS channels 7-14 are modified by adding the alternating Fourier series (2) in the orbital angle.

AltFourierCh6-11: As AltFourierCh6-13, but adding the alternating Fourier series to the bias correction models of channels 6-11 of AMSU-A and 7-12 of ATMS only.

AltFourierCh5-9: As AltFourierCh6-13, but adding the alternating Fourier series to the bias correction models of channels 5-9 of AMSU-A and 6-10 of ATMS only.

In all of these experiments, the bias correction model for channels 14 of AMSU-A (15 of ATMS) remains unchanged. This is to avoid altering the anchoring provided by using Constrained VarBC for the top-most channel to stabilise the temperature analysis in the stratosphere (Han and Bormann 2016).

All experiments cover the periods 2 June – 31 August 2020 and 2 December 2020 – 28 February 2021. They use ECMWF’s 12-hour 4-dimensional variational assimilation (4D-Var) system with a spatial model resolution of T_{CO399} (≈ 25 km), a final incremental analysis resolution of $T_L 159$ (≈ 125 km), and 137 levels in the vertical. Background errors of the day are specified through a 50-member Ensemble of Data Assimilations (EDA), combined with a climatological background error; the background error is the same in all five experiments.

3.3 Results

3.3.1 Analysis impact

As expected, with the orbital bias correction terms added, VarBC is able to reduce the residual orbital bias significantly (e.g., Fig. 11). The residual orbital bias is now small compared to the standard deviation of background departures for both the 5-th order Fourier series as well as the alternating Fourier series

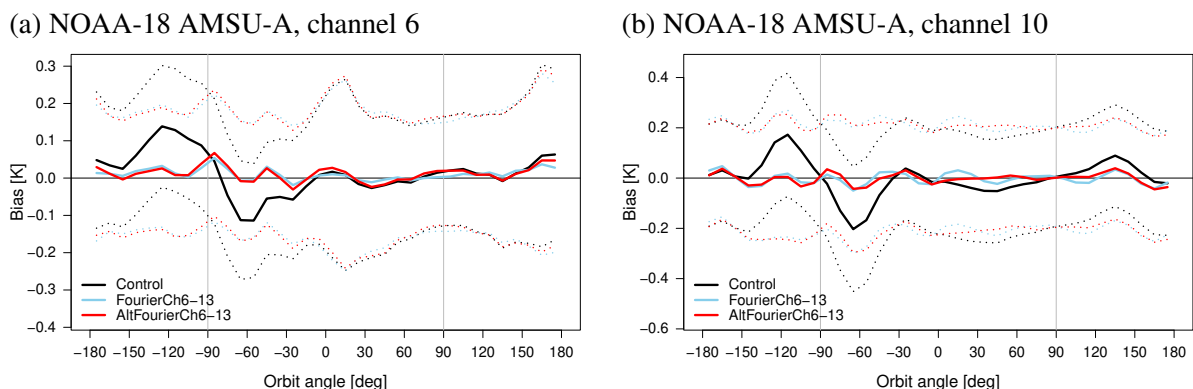


Figure 11: Residual bias (solid line) for assimilated NOAA-18 AMSU-A observations from channel 6 (a) and channel 10 (b) as a function of orbital angle for August 2020, for the three experiments as shown in the legend. Dotted lines depict plus/minus one standard deviation of the background departures (after bias correction) around the residual bias.

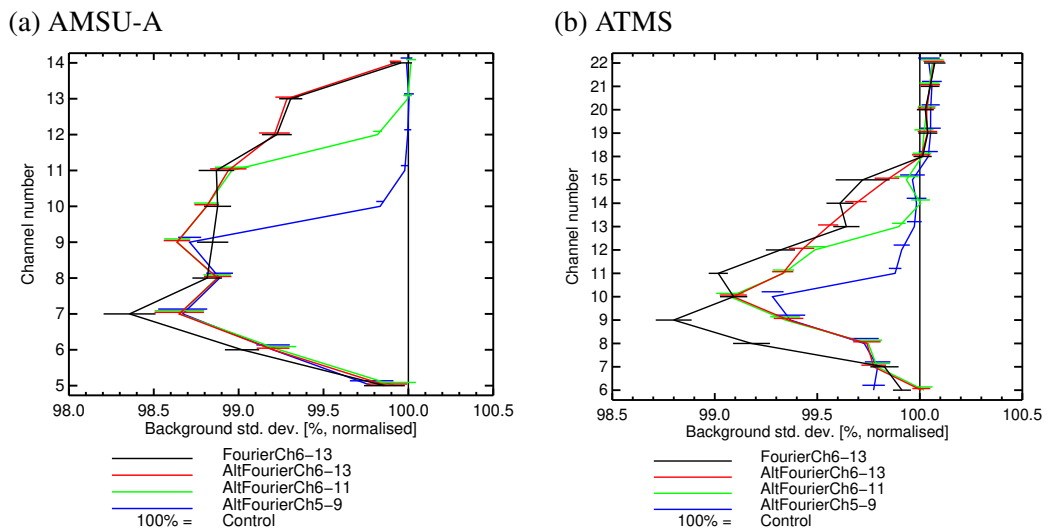


Figure 12: a) Standard deviation of the background departures of all used AMSU-A data (after bias correction) for the experiments considered in this study (see legend), normalised by values from the Control. Results for the two seasons have been combined. b) As a), but for ATMS.

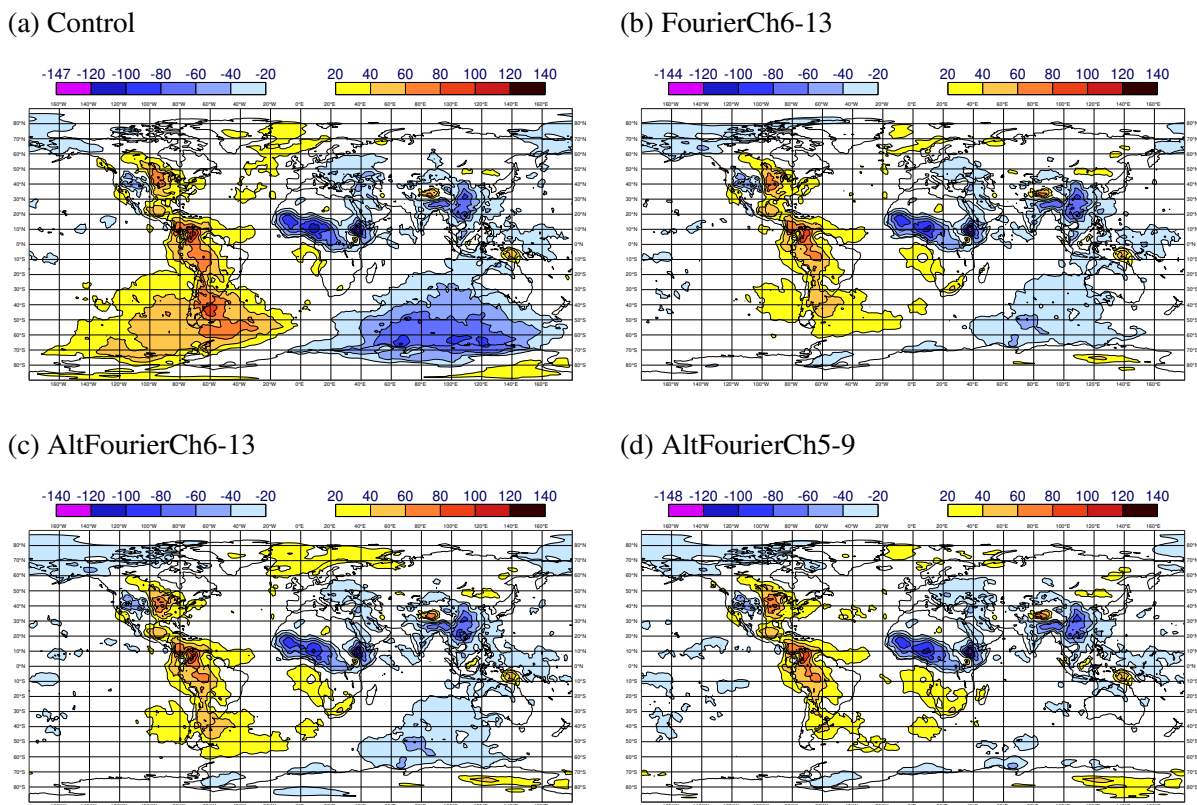


Figure 13: Difference in the mean increments between the 12Z and the 0Z cycle for the 925-200 hPa geopotential thickness $[m^2/s^2]$ for June-August 2020. The different panels show results for the Control (a), and three experiments with orbital bias correction as indicated.

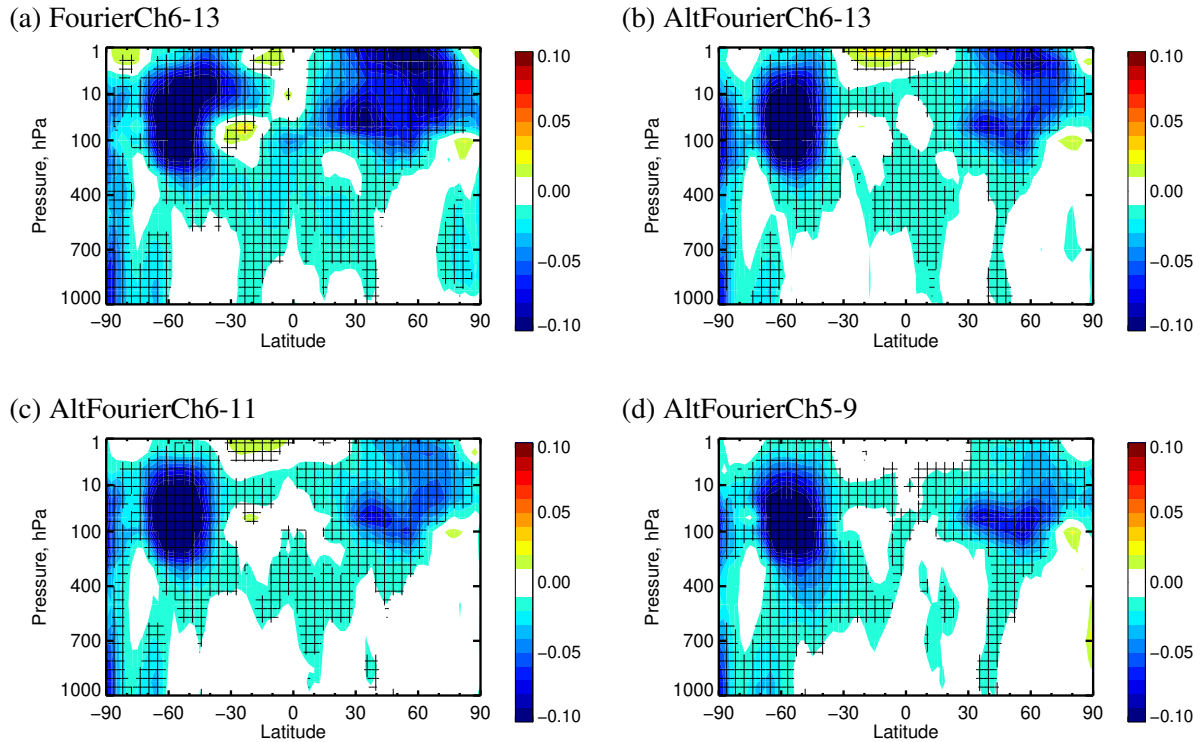


Figure 14: Normalised difference in the zonal mean root-mean-squared (RMS) increment in the geopotential between the experiment indicated above the panel and the Control. Statistics for both seasons have been combined.

alternative. The bias coefficients spin-up relatively quickly (typically within 2-3 days), and after that they change slowly over time (not shown), as expected from the temporal evolution of the orbital biases noted earlier.

The reduction in the residual orbital bias is reflected in a reduction in the standard deviation of background departures for the affected channels (Fig. 12). The size of the latter is dependent on the season and hemisphere as expected from previous characterisation, and it reaches, for instance, a sizeable 6 % for AMSU-A channel 7 over the Southern Hemisphere for the June-August period. For AMSU-A, the reduction in the standard deviation of background departures is similar for the FourierCh6-13 and the AltFourierCh6-13 experiment (the reduction is slightly smaller for channels 6 and 7 in AltFourierCh6-13 and slightly larger for channel 9). This suggests that both models are indeed similarly effective. For ATMS, the reduction in the standard deviation of background departures is not as pronounced for AltFourierCh6-13.

The reduction in the orbital biases leads to a significant reduction in the systematic diurnal increments that first prompted this study for all of the correction experiments considered here (cf Fig. 13b-d with Fig. 13a). This is particularly the case when the orbital bias correction is also applied to channel 5 of AMSU-A (and channel 6 of ATMS), a channel that has a weighting function peak at around 600 hPa. In this case the significant increment differences visible over the Southern Hemisphere are completely removed (Fig. 13d), whereas small differences remain when this channel is not included in the orbital bias correction (Fig. 13b, c). More generally, the smaller departures for AMSU-A and ATMS lead to an overall reduction in the size of the increments for a range of variables, as shown, for instance for the geopotential in Fig. 14. The reduction is largest over the mid- and higher latitudes and over the upper troposphere/ lower stratosphere. Below around 50 hPa the reduction in the size of the increments is

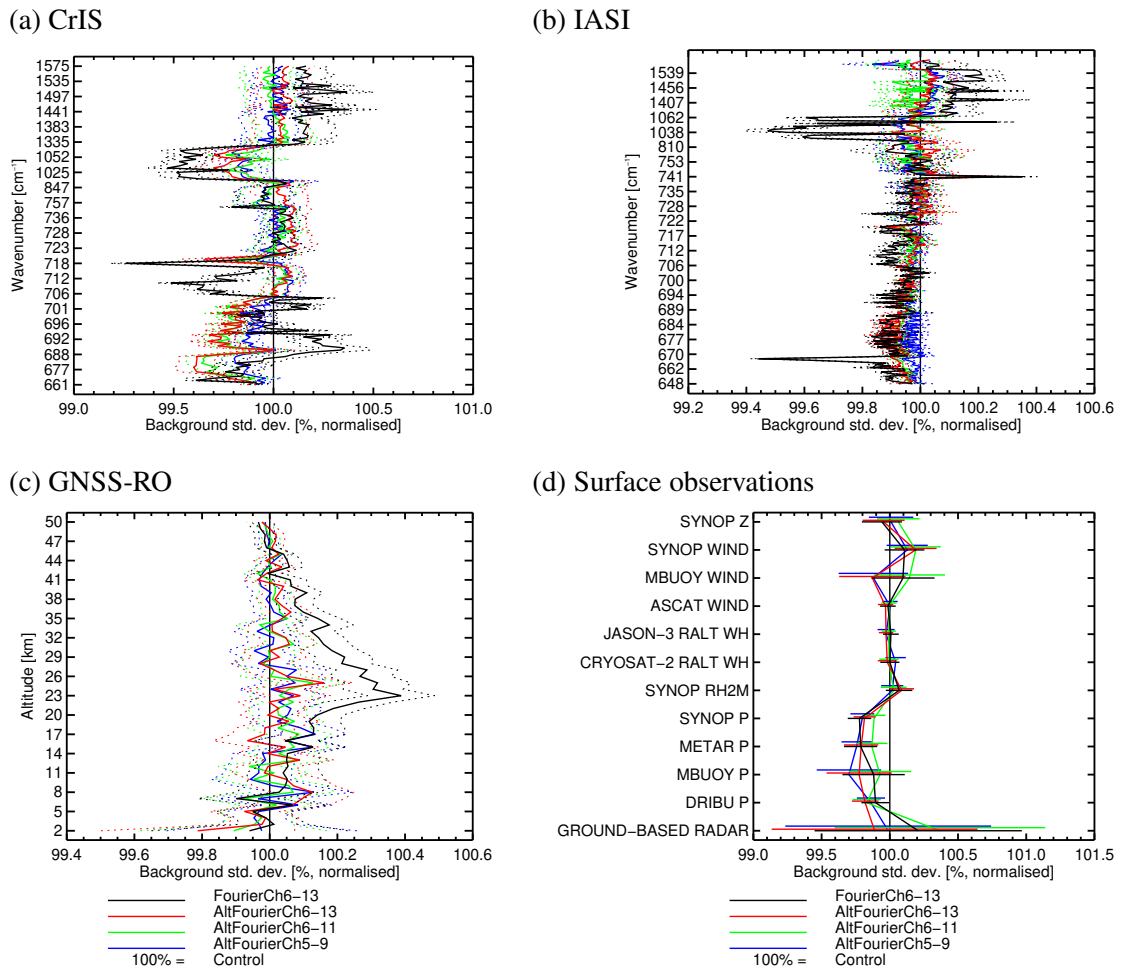


Figure 15: a) Standard deviation of the background departures of used CrIS data (after bias correction) for the experiments considered in this study (see legend), normalised by the Control. Results for the two seasons have been combined. b) As a), but for IASI. c) As a), but for GNSS-RO observations. d) As a), but for near-surface observations.

similar for the four experiments considered, whereas some differences are visible above this level. The reduced increments indicate a greater self-consistency of the assimilation system, which is considered a positive aspect.

Examining the effect of the orbital bias correction on the size of background departures of other observations reveals notable differences in the performance of the FourierCh6-13 experiment compared to the experiments with the alternating Fourier series (Fig. 15). All experiments show reduced standard deviations of background departures for some of the stratospheric temperature channels of CrIS and IASI (Fig. 15a and b) and for mean-sea-level pressure measurements from a range of observations (Fig. 15d). This shows a better agreement between the short-range forecasts and the observations, suggesting an improved forecast accuracy for these aspects. However, the FourierCh6-13 experiment shows also some degradations, such as for radio-occultation observations in the stratosphere or humidity-sounding channels of CrIS and IASI (wavenumber range 1335-1575 cm^{-1} , see black line in Fig. 15). For these observations, standard deviations of analysis departures are also increased (not shown). The degradations are absent when the alternating Fourier series is used instead (see other coloured lines in Fig. 15), and the

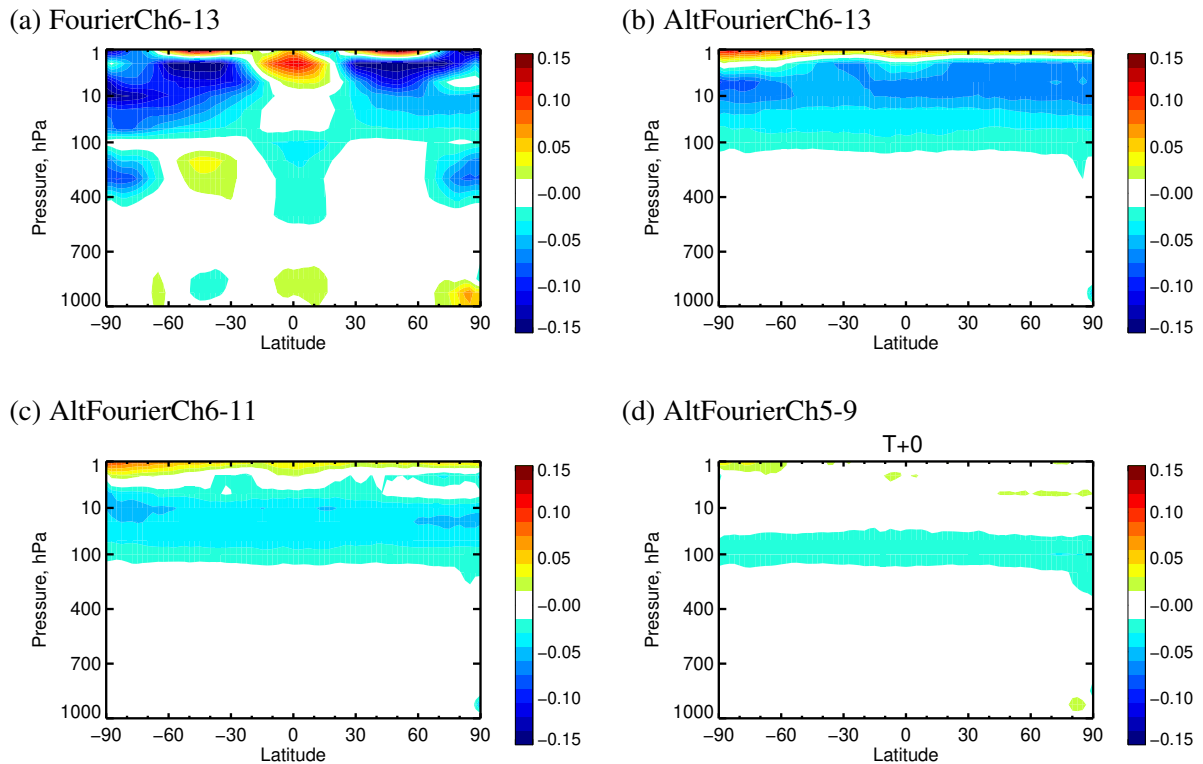
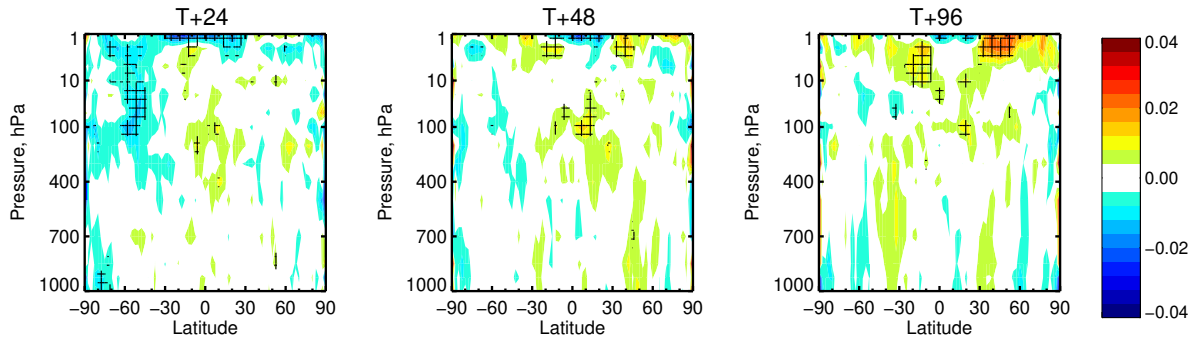


Figure 16: Difference in the zonal mean analysed temperature [K] between the experiment indicated above the panel and the Control. Statistics for both seasons have been combined.

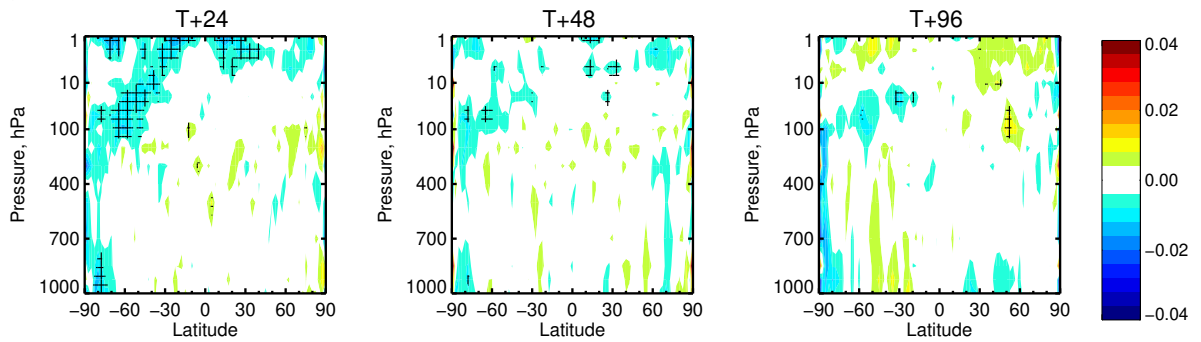
performance is more neutral in this respect, particularly when the correction is applied to fewer channels. It appears that some of the modifications introduced through the bias correction with the largest number of degrees of freedom in FourierCh6-13 are not supported by the rest of the observing system.

Digging further into the slightly different performance depending on the bias correction model, it is notable that FourierCh6-13 exhibits more complex changes in the mean analyses than the other experiments, as highlighted in terms of the zonal mean temperature differences in Fig. 16. All experiments show some differences in the mean analysis over the stratosphere. But the magnitude of the changes is largest in FourierCh6-13, and the changes exhibit some zonal structure and extend into the troposphere (Fig. 16a). In contrast, the changes in the mean analysis are globally relatively constant and primarily confined to above 100 hPa when the more restrictive alternating Fourier series is used (Fig. 16b). Avoiding additional degrees of freedom to correct for biases with zonal structure was one of the motivations for using the alternating Fourier series, and it appears that this indeed behaves as expected. The changes in the mean analysis are likely the result of interaction between model bias in the stratosphere, VarBC and the estimation of model bias through weak-constraint 4D-Var (Laloyaux et al 2020). The size of the model bias diagnosed through the weak-constraint formulation is nevertheless largely unaffected (not shown). While the size of the changes is relatively small in terms of temperature (up to 0.15 K in the case of FourierCh6-13), they are not supported by other observations such as temperature observations from radiosondes or bending angles from radio-occultation measurements (not shown). The size of the change can be further reduced when the orbital bias correction is not applied to the highest-peaking stratospheric channels (Fig. 16c, d), albeit at the expense of reduced benefit in the standard deviations of background departures for the affected AMSU-A and ATMS channels, as seen in Fig. 12.

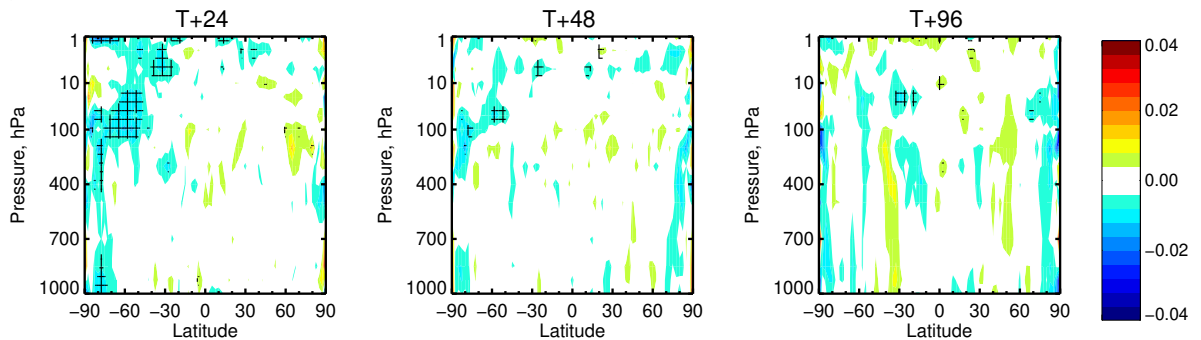
(a) FourierCh6-13



(b) AltFourierCh6-13



(c) AltFourierCh6-11



(d) AltFourierCh5-9

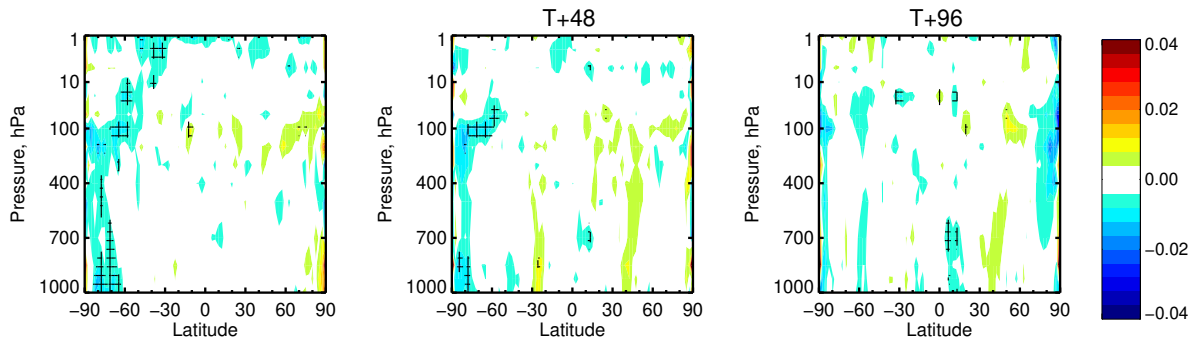


Figure 17: a) Zonal mean of the normalised difference in the RMS of the wind forecast error between the FourierCh6-13 experiment and the Control for the day 1, 3, and 5 forecast error. Each experiment has been verified against its own analysis and statistics for both seasons have been combined. b) As a), but for the AltFourierCh6-13 experiment. c) As a), but for the AltFourierCh6-11 experiment. d) As a), but for the AltFourierCh5-9 experiment.

3.3.2 Forecast impact

Finally, we can also consider the forecast impact of the orbital bias correction into the medium-range. Figure 17 shows the zonal mean of the normalised difference in the RMS of the wind forecast error at different forecast ranges as an example; the performance for other variables is similar. When each experiment is verified against its own analysis, some reduction in the forecast error can be seen for all four experiments at day 1, linked to the reduced increments and better self-consistency noted earlier. For the FourierCh6-13 experiment, degradations in the forecast impact start to prevail in the stratosphere from about day 2 onwards. In contrast, the experiments with the alternating Fourier series perform better in this respect, with the AltFourierCh6-11 and the AltFourierCh5-9 exhibiting a neutral to slightly positive forecast impact. Some benefits appear to last out to day 2 in the troposphere at high southern latitudes in AltFourierCh5-9, but magnitudes remain small. Again, it appears that the more restrictive bias correction used in the experiments with the alternating Fourier series performs better, presumably as it avoids overfitting air-mass dependent biases, some of which may not be observation-related biases.

4 Conclusions

In this memorandum we have characterised orbital biases in temperature-sounding channels of AMSU-A and ATMS in the ECMWF system, and experimented with a modification to the bias correction for the affected channels to address the orbital biases during the assimilation. The main findings are:

- The AMSU-A and ATMS temperature-sounding channels exhibit considerable residual orbital biases compared to short-range forecast equivalents from the ECMWF system when the standard operational bias correction is applied. The magnitude can be of similar size as the instrument noise for the affected channels (0.1-0.2 K) and thus of a similar size as the random errors in the background.
- The magnitude of the orbital bias varies with satellite/instrument, with AMSU-A on NOAA-18 exhibiting the strongest bias. The bias shows distinct seasonal pattern, with largest biases in June-October positioned over the Southern Hemisphere. For AMSU-A, the shape of the bias as a function of orbit angle is similar for different channels, and the seasonal patterns are remarkably similar for different instruments, despite very different equator-crossing times and hence thermal environments on the satellite.
- The orbital biases cause systematic diurnal increments in the 12-hourly ECMWF analyses, most noticeable during the June-August period over the Southern Hemisphere. These systematic diurnal increments are not present if MW sounders are removed from the assimilation system, and the diurnal biases are not present in other observations with similar sensitivity. While the root-cause of the orbital bias is not clear, indications are that the bias is observation-related, rather than a bias in the background.
- The orbital biases and hence the systematic diurnal increments in the ECMWF system can be successfully reduced significantly through a modification of the bias correction model for the affected channels. The modified bias correction applies either a 5th-order Fourier series in the orbital angle as model for the orbital bias, or a more restricted alternating Fourier series.
- Adding the 5-th order Fourier series to the bias model leads to a change in the bias of the temperature analysis in the stratosphere with larger effects at high-latitudes, and these changes are not

supported by other observations. The changes in the mean analysis can be controlled by using instead the alternating Fourier series to model the orbital biases and by not applying the orbital bias correction to the stratospheric channels.

- Correcting the orbital biases with the alternating Fourier series leads to reduced increments and minor benefits in the short-range forecasts as seen against other observations, but only marginal forecast benefits beyond day 2.

The present study has highlighted that even well-used and established satellite observations can exhibit biases that have so far remained uncharacterised and whose origin is difficult to understand. This in turn also highlights the gradual improvement in NWP systems and their ability to detect even minor biases that a couple of decades ago were not detectable and likely did not matter in the assimilation of AMSU-A data at the time. The study illustrates the benefit of revisiting assimilation choices for established observations, in order to keep them in step with improvements in the overall forecasting system. Detailed diagnostics and monitoring efforts are important to detect such biases and to enable revisions of the assimilation choices.

Further work is required to determine the root-cause of the orbital bias for AMSU-A and ATMS temperature-sounding channels. While there are some indications that it may be linked to neglected variations in the calibration (e.g., of the cold-space correction, see appendix A.2), the relatively small size of the bias compared to other bias contributions makes any root-cause attribution difficult. Nevertheless, it would be interesting to forward model neglected effects in the calibration and establish whether these match some of the characteristics found in the present work. Such investigations are best done in close collaboration between instrument and calibration experts at space agencies or other organisations and NWP data scientists. Furthermore, comparison with orbital bias statistics from other NWP systems could be informative. In this context, it is possible that the ECMWF system with its 12-hour assimilation window may be more exposed to the orbital biases, as it makes increments with diurnal patterns particularly apparent. Other NWP centres employ 6-hour (or even shorter) windows, and this will affect the increment pattern as well as the appearance of the orbital bias.

The benefit demonstrated in this memorandum from applying the orbital bias correction needs to be weighed up against the added complexity when deciding about the future operational application of the scheme. The orbital bias correction successfully removes the systematic increments that first prompted this investigation, leads to small forecast benefits in the short range, and the reduced size of the background departures should enhance the ability to detect and diagnose other errors in the background for the instruments affected in the future. On the other hand, the scheme adds complexity to the bias correction, and there is potential for interaction with model bias which may change with the evolution of the forecast model or treatment of model bias. In this context, the present work has highlighted the benefit of using the more restricted orbital bias correction model based on the alternating Fourier series and applied to tropospheric/lower stratospheric channels only. The restriction to the lower sounding channels means that good anchor observations are available, therefore helping to constrain the bias correction. Further motivations for applying the scheme to AMSU-A and ATMS data come from reanalyses, for which the removal of systematic diurnal increments may be relevant to specific evaluations of diurnal aspects. In this context, it is worth recalling that the ERA5 reanalysis shows systematic diurnal increments also prior to the advent of AMSU-A (Fig. 2), so orbital biases may also be present in the data from the TOVS era, an aspect that would be worth investigating further. For now, the configuration tested here in the experiment AIFourierCh5-9 is planned for implementation in cycle 49r2 of the ECMWF assimilation system.

Aside from the application to AMSU-A and ATMS data, the orbital bias correction investigated here

could be applied to correct orbital biases in other satellite data. This is provided the bias as a function of orbital angle only evolves slowly in time, and does not exhibit very sharp features. Features that change sharply with the orbital angle will be difficult to fit with a Fourier-series-based prediction model and may require more tailored bias predictors. Examples of observations which are currently not assimilated at ECMWF due to orbital biases are the Chinese MWRI instrument or the temperature-sounding channels on SSMI/S (e.g., Scanlon et al 2023, Bell et al 2008). These observations could be re-evaluated with the new orbital bias correction added. In the future, MW radiances from cube-sats or small satellites may be more prone to orbital biases than data from large satellites, given the more limited capabilities to control the thermal environment. The orbital bias correction investigated here may become a critical element in the successful use of such data.

A Appendix

A.1 Bias characteristics versus orbital angle for other instruments

The orbital bias pattern seen in AMSU-A and ATMS observations are not supported by other observations present in the ECMWF system. This was already pointed out in the context of the increment pattern discussed in the introduction and the finding that the systematic diurnal increments are not present in experiments for which the MW sounders are denied (Fig. 3). To further cross-check this aspect we can also directly investigate bias pattern from other instruments. To this end, Fig. 18 shows residual biases as a function of time and orbital angle for selected channels on a IASI, CrIS, and the MWHS-2 instrument. IASI and CrIS are two hyperspectral infrared instruments, whereas MWHS-2 is a MW sounder with channels in the 118 and 183 GHz bands. The 118 GHz bands on MWHS-2 are interesting in this context as they provide further passive MW measurements around an oxygen line, but for a different frequency than the channels on AMSU-A and ATMS. The channels shown peak at similar altitudes as channels 6 and 10, to allow comparison with Figures 6 and 8. In particular, Figures 6a and b and 18a and b provide results from the same satellite platform thus with the same overpass times, as do Figures 8a and b and 18c and d.

While there are seasonally varying biases present in all of the channels shown in Fig. 18, the patterns are very different from the ones seen for AMSU-A and ATMS. For the two infrared instruments, the biases also tend to be smaller than those observed for their MW counterparts, and they are locally symmetric around $\pm 90^\circ$. The latter suggests that these are likely residual air-mass dependent biases with zonal structure, different from the ones seen for AMSU-A and ATMS. Note in this context the change in the bias characteristics in July 2020 which is caused by the operational implementation of cycle 47r1 which affected the data selection for these channels. For MWHS-2, some dipole structure may be present in channel 6 around July for some of the years, with negative biases around $\beta = 40^\circ$ and positive biases around 140° . This has some resemblance to patterns seen in the Metop-A channel 6, peaking at the same altitudes (cf Fig. 6c), but the magnitudes are different. Note that in general the residual bias seen for MWHS-2 channels 3 and 6 is relatively large in comparison to similar channels on AMSU-A or ATMS. But for these channels the instrument noise and the assigned observation error are also much larger, so these biases are less important in the assimilation (assigned clear-sky observation errors over sea are 1.0 K for MWHS-2 channel 6 versus 0.17-0.32 for AMSU-A channel 6, and they are 1.2 K for MWHS-2 channel 3 versus 0.25-0.27 K for AMSU-A channel 10).

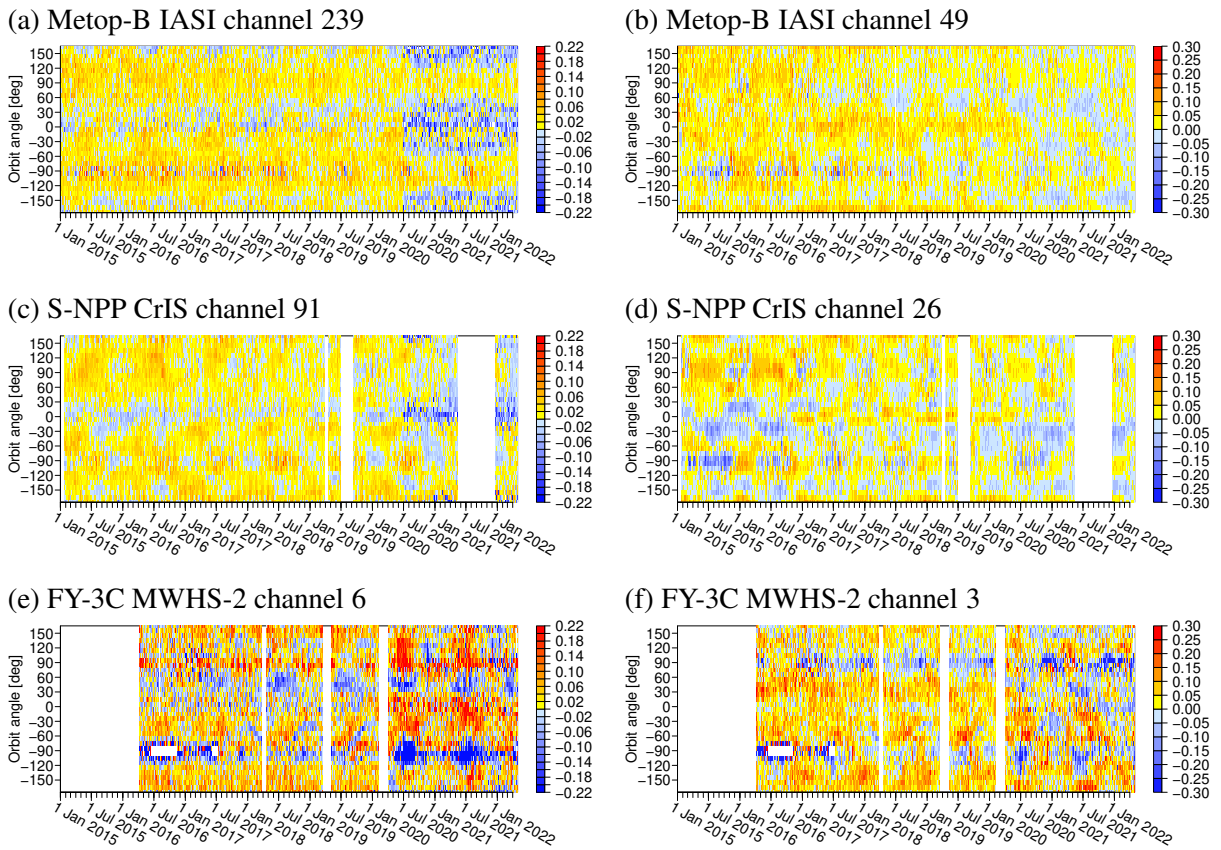


Figure 18: As Fig. 6, but for selected different instruments and channels that peak at altitudes similar to AMSU-A channel 6 and 10. The three rows give statistics for Metop-B IASI, S-NPP CrIS, and the FY-3C MWHS-2, respectively. Results for channels that peak at similar altitudes to AMSU-A channel 6 are shown in the left column, whereas results for channels peaking at similar altitudes as AMSU-A channel 10 are shown in the right column, with channels numbers given in the panel heading.

A.2 Scene-temperature dependence of orbital biases

To further analyse the characteristics of the orbital biases, we have considered its dependence on the scene temperature for the AMSU-A instruments. This is to investigate whether the bias can be linked to particular aspects of the instrument’s calibration. AMSU-A uses a two-point calibration to convert measured counts into antenna temperatures, based on viewing cold space and a warm calibration target with a known temperature (e.g., Mo 2008, Yan et al 2020). For the cold-space temperature, a correction is applied to take into account contaminations from the space-craft or the Earth’s limb through antenna side-lobes, adding around 2 K to the cosmic background of 2.73 K. This correction is assumed to be fixed and any variations in the Earth-limb temperature or the space-craft are neglected. Non-linearities of the receiver are addressed through a non-linearity correction based on pre-launch measurements (e.g., Mo 1996). Sub-optimality in either of these aspects, such as neglected orbital variations, will result in biases that are dependent on the scene temperature.

Figure 19 shows the bias for NOAA-18 AMSU-A in August 2020 as a function of the average of the observed and simulated brightness temperature. Panels a and b show residual biases after bias correction for orbit-angle ranges with prominent biases for this period. There is indeed considerable dependence of the residual bias on the scene-temperature, with largest absolute biases around a brightness temper-

ature of 200-220 K (depending on channel), whereas globally the scene-temperature dependence of the residual bias is small (Fig. 19c). If neglected variations in the cold-space correction were indeed the cause, we would expect to see larger positive or negative biases with decreasing brightness temperatures in panels a and b, with values near zero around the warm-calibration point (around 287 K). It is clear that the scene-temperature dependence of the bias is more complex than that and that additional mechanisms must hence be at work. Nevertheless, the statistics shown suggest that a variation in the cold-space correction of a few tenths of K would help to reduce the residual bias for the two orbit-angle ranges shown, so this aspect may be a relevant contribution.

In this context, Figures 19d-f highlight a key issue with any attempt of attributing the orbital biases: compared to the biases before bias correction, the residual orbital biases are relatively small. It is clear that the orbital bias is mixed with a range of other biases, and its small size makes it very difficult to disentangle it from these other biases. Aside from potential short-comings in the calibration or the antenna-pattern correction (Mo 1999), radiative-transfer biases are thought to contribute significantly to these overall biases. Lu and Bell (2014), for instance, show that overall biases and their variations can be significantly reduced for AMSU-A by using channel pass-bands in the radiative transfer calculations that

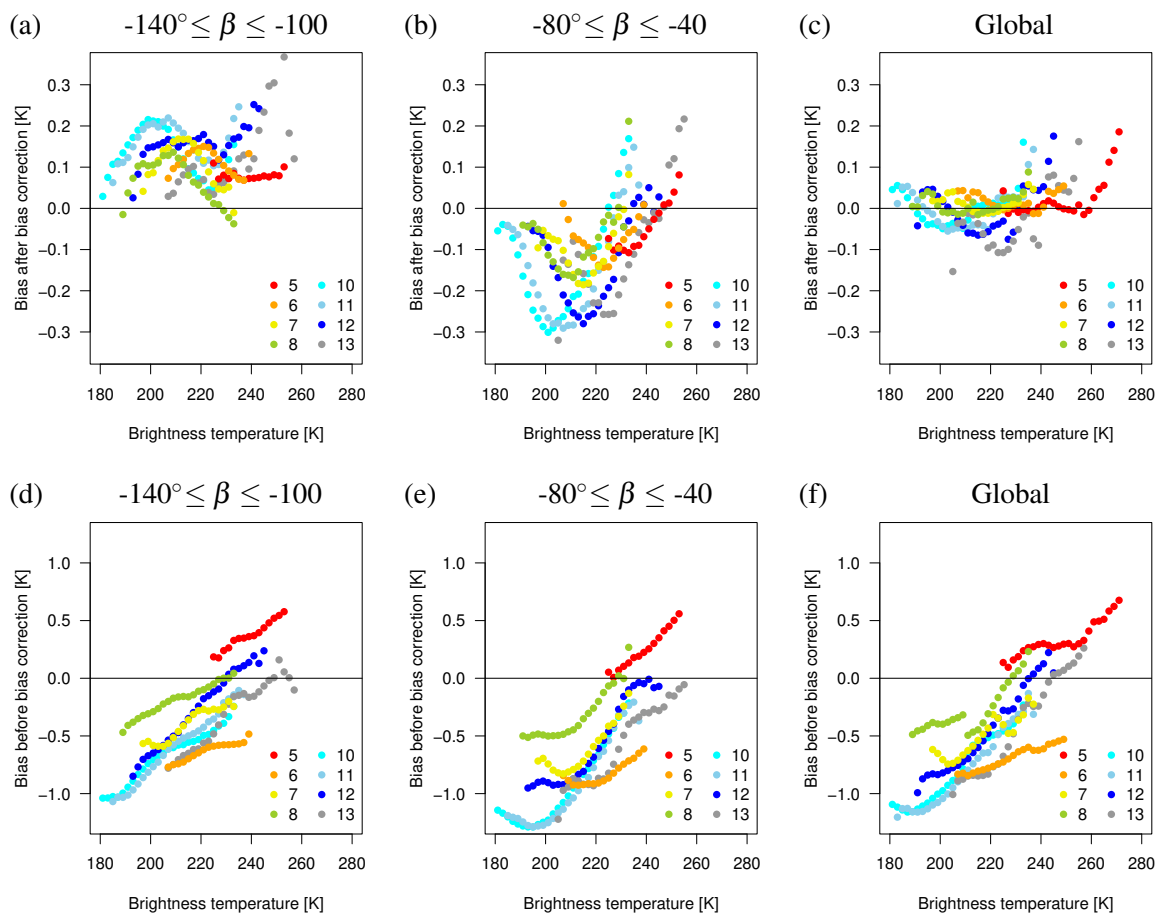


Figure 19: a) Residual bias for NOAA-18 AMSU-A used observations as a function of the average between the observed and the background brightness temperature. Different colours indicate different channels, with channel numbers indicated in the legend. Statistics are for August 2020, for the area with $-140^\circ \leq \beta \leq -100$. b) As a, but for $-80^\circ \leq \beta \leq -40$. c) As a, but for all used data. Panels d-f show equivalent statistics to panels a-c, but for the bias before bias correction.

are shifted compared to the specified values. VarBC will attempt to correct for the overall combination of such radiative transfer and calibration-related biases, but its ability to do so is affected, among other things, by the assumed bias models and potential model biases. The residual biases are hence unlikely to show a “clean” signature of the leading cause of the orbital bias, but rather one in which some aspects have already been corrected, depending on how well the bias patterns map onto the current empirical bias model or to what extent the biases are affected by model bias. A possible way to make further progress in understanding the biases would be a metrological approach that aims to forward model systematic errors in the instrument, the calibration and the radiative transfer (e.g., Yang et al 2023), combined with an analysis how VarBC deals with such biases.

Acknowledgements

Discussions with and input from Jörg Ackermann (EUMETSAT), Nigel Atkinson (Met Office), Bill Bell (ECMWF), Robin Faulwetter (DWD), Hu Tiger Yang (UMD/CISESS), and John Xun Yang (UMD/ESSIC) on the orbital bias characteristics and their potential origins are gratefully acknowledged.

References

- A.P.McNally, and G. Kelly, 1999: The use of raw tovs/atovs radiances in the ecmwf 4d-var assimilation system. In Proceedings of the ECMWF/EUMETSAT Workshop on Use of ATOVS Data for NWP Assimilation, ECMWF, 23–32.
- Bell, W., S. English, B. Candy, N. Atkinson, F. Hilton, N. Baker, S. Swadley, W. Campbell, N. Bormann, G. Kelly, and M. Kazumori, 2008: The assimilation of SSMIS radiances in Numerical Weather Prediction models. *IEEE Trans. Geosci. Remote Sensing*, **46**, 884–900.
- Booton, A., W. Bell, and N. Atkinson, 2013: An improved bias correction for ss-mis. In Proceedings of the 19th International TOVS Study Conference, ITWG, https://cimss.ssec.wisc.edu/itwg/itsc/itsc20/papers/11_02_booton_paper.pdf.
- Bormann, N., and P. Bauer, 2010: Estimates of spatial and inter-channel observation error characteristics for current sounder radiances for NWP, part I: Methods and application to ATOVS data. *Q. J. R. Meteorol. Soc.*, **136**, 1036–1050.
- Bormann, N., and M. Bonavita, 2013: Spread of the ensemble of data assimilations in radiance space. Technical Memorandum 708, ECMWF, Reading, UK, 29 pp [available under www.ecmwf.int/publications/library/do/references/list/14].
- Bormann, N., A. Fouilloux, and W. Bell, 2013: Evaluation and assimilation of ATMS data in the ECMWF system. *J. Geophys. Res.*, **118**, 12,970–12,980, doi: 10.1002/2013JD020325.
- Bormann, N., H. Lawrence, and J. Farnan, 2019: Global observing system experiments in the ECMWF assimilation system. Technical Memorandum 839, ECMWF, Reading, UK.
- Dee, D., 2004: Variational bias correction of radiance data in the ECMWF system. In ECMWF Workshop on Assimilation of High Spectral Resolution Sounders in NWP, ECMWF, Reading, UK, 97–112.
- Duncan, D., N. Bormann, A. Geer, and P. Weston, 2022: Assimilation of AMSU-A in all-sky conditions. *Mon. Wea. Rev.*
- Geer, A., P. Bauer, and N. Bormann, 2010: Solar biases in microwave imager observations assimilated at ECMWF. *IEEE Trans. Geosci. Remote Sensing*, **48**, 2660–2669.

- Han, W., and N. Bormann, 2016: Constrained adaptive bias correction for satellite radiance assimilation in the ecmwf 4d-var system. *ECMWF Technical Memorandum*, 783.
- Hersbach, H., W. Bell, P. Berrisford, S. Hirahara, A. Horányi, J. Muñoz-Sabater, J. Nicolas, C. Peubey, R. Radu, D. Schepers, A. Simmons, C. Soci, S. Abdalla, X. Abellan, G. Balsamo, P. Bechtold, G. Biavati, J. Bidlot, M. Bonavita, G. De Chiara, P. Dahlgren, D. Dee, M. Diamantakis, R. Dragani, J. Flemming, R. Forbes, M. Fuentes, A. Geer, L. Haimberger, S. Healy, R. Hogan, E. Hólm, M. Janisková, S. Keeley, P. Laloyaux, P. Lopez, C. Lupu, G. Radnoti, P. de Rosnay, I. Rozum, F. Vamborg, S. Villaume, and J.-N. Thépaut, 2020: The era5 global reanalysis. *Q. J. R. Meteorol. Soc.*, **146**, 730, 1999–2049.
- Laloyaux, P., M. Bonavita, M. Dahoui, J. Farnan, S. Healy, E. Hólm, and S. Lang, 2020: Towards an unbiased stratospheric analysis. *Q. J. R. Meteorol. Soc.*, **146**, 730, 2392–2409.
- Lu, Q., and W. Bell, 2014: Characterizing channel center frequencies in AMSU-A and MSU microwave sounding instruments. *J. Atmos. Oceanic Technol.*, **31**, 1713–1732.
- Mo, T., 1996: Prelaunch calibration of the advanced microwave sounding unit-a for noaa-k. *IEEE Transactions on Microwave Theory and Techniques*, **44**, 8, 1460–1469.
- Mo, T., 1999: Amsu-a antenna pattern corrections. *IEEE Transactions on Geoscience and Remote Sensing*, **37**, 1, 103–112.
- Mo, T., 2008: Postlaunch calibration of the metop-a advanced microwave sounding unit-a. *IEEE Transactions on Geoscience and Remote Sensing*, **46**, 11, 3581–3600.
- Saunders, R., J. Hocking, E. Turner, P. Rayer, D. Rundle, P. Brunel, J. Vidot, P. Roquet, M. Matricardi, A. Geer, N. Bormann, and C. Lupu, 2018: An update on the RTTOV fast radiative transfer model (currently at version 12). *Geosci. Model Dev.*, **11**, 2717–2737, <https://doi.org/10.5194/gmd-11-2717-2018>.
- Scanlon, T., A. Geer, and N. Bormann, 2023: Microwave imagers in the ecmwf-ifs: Adding further observations and improving convective anvils in the observation operator. EUMETSAT/ECMWF Fellowship Programme Research Report 61, ECMWF, 36 pp.
- Xie, X., S. Wu, H. Xu, W. Yu, J. He, and S. Gu, 2019: Ascending–descending bias correction of microwave radiation imager on board fengyun-3c. *IEEE Transactions on Geoscience and Remote Sensing*, **57**, 6, 3126–3134.
- Yan, B., J. Chen, C.-Z. Zou, K. K. Ahmad, H. Qian, K. Garrett, T. Zhu, D. Han, and J. Green, 2020: Calibration and validation of antenna and brightness temperatures from Metop-C Advanced Microwave Sounding Unit-A (AMSU-A). *Remote Sens.*, **12**(18), 2978; doi.org/10.3390/rs12182978.
- Yang, J., Y. You, W. Blackwell, C. Da, C. Grassotti, Q. Liu, R. Ferraro, H. Meng, C.-Z. Zou, S.-P. Ho, J. Yin, V. Petkovic, T. Hewison, D. Posselt, A. Gambacorta, D. Draper, S. Misra, R. Kroodsma, and M. Chen, 2023: SatERR: A community error inventory for satellite microwave observation error representation and uncertainty quantification. *Bull. Amer. Meteor. Soc.*, doi.org/10.1175/BAMS-D-22-0207.1, in press.